Applied Catalysis B: Environmental 130–131 (2013) 106–111

Contents lists available at SciVerse ScienceDirect

Applied Catalysis B: Environmental

journal homepage: www.elsevier.com/locate/apcatb

Anti-bacterial activity of indoor-light activated photocatalysts

Damian W. Synnott[a,b], Michael K. Seery[b], Steven J. Hinder[c], Georg Michlits[b], Suresh C. Pillai[a,*]

[a] Centre for Research in Engineering Surface Technology (CREST), FOCAS Institute, Dublin Institute of Technology, Camden Row, Dublin 8, Ireland
[b] School of Chemical and Pharmaceutical Sciences, Dublin Institute of Technology, Kevin St. Dublin 8, Ireland
[c] The Surface Analysis Laboratory, Faculty of Engineering and Physical Sciences, University of Surrey, GU2 7XH, United Kingdom

ARTICLE INFO

Article history:
Received 29 May 2012
Received in revised form 16 October 2012
Accepted 22 October 2012
Available online 1 November 2012

Keywords:
Gram positive and gram negative bacteria
Decontamination
Visible light
XPS
Solar
Anti-microbial
ZnO
MRSA
Green and energy efficient synthesis
Anti-MRSA coatings
Hospital acquired infections
Photo-activity
Emerging pollutants
TiO_2
Degussa P-25
Cell wall
Disinfection
Micro-biology
Doping
Band gap
Escherichia coli
P. aerginosa
Methicillin-resistant *Staphylococcus aureus* (MRSA)

ABSTRACT

Nanocrystalline photocatalysts, prepared under ambient conditions using a microwave assisted synthesis, show indoor light photocatalytic activity for the degradation of *Staphylococcus aureus* and *Escherichia coli*. The zinc sulphide (ZnS) nanomaterials, prepared by a microwave assisted synthesis, are shown to be cubic blende structure with an average crystallite size of 4–6 nm. The anti-bacterial activity of these nanomaterials is investigated under irradiation from a 60 W light bulb and photocatalytic activity is revealed to be due to the defects present in the crystal structure. The ZnS shows anti-bacterial action as both a bacteriostatic and bacteriocidal (88% reduction in the amount of bacteria in 5 h) material and the methods of bacterial degradation on the ZnS is discussed. The anti-bacterial actions of these materials were also compared with commercial ZnS and Evonik-Degussa P-25. A detailed mechanism for the light absorption in the visible light region of the microwave prepared ZnS is proposed based on the luminescence spectroscopy.

1. Introduction

Semiconductor photocatalysis has been shown to be an effective method of removing bacterial contamination, including *Escherichia coli* and *Staphylococcus aureus*, in hospitals and in the food industry. [1–9] Zinc sulphide is an important II–VI semiconductor with a band gap of 3.8 eV. [10,11] Zinc sulphide has a great potential as an anti-bacterial semiconductor due to its relatively deeper conduction and valence bands compared to other semiconductors including TiO_2 and ZnO [3,12]. The comparatively negative positions of the conduction and valence bands of ZnS *versus* the NHE are located at −2.3 and +1.4 eV respectively. ZnS was one of the first semiconductors discovered and is of major interest in biomedical, electronic and photovoltaic devices due to its luminescent and catalytic properties [13,14]. It has been used as an important component in ultraviolet light emitting diodes [15], injection lasers, flat panel displays [16], solar cells [17], and as a photocatalysts in many situations including a visible light activated water-splitting agent [18].

ZnS has been synthesised in a number of ways including by precipitation method [19], by spray pyrolysis [20], by hydrothermal synthesis [21], in solution [22], using ligands [23], with conjugated

* Corresponding author.
E-mail address: suresh.pillai@dit.ie (S.C. Pillai).

0926-3373/$ – see front matter © 2012 Elsevier B.V. All rights reserved.
http://dx.doi.org/10.1016/j.apcatb.2012.10.020

polymers [24], using ultrasonic irradiation [25], and employing microwave heating [26]. Microwave heating as a synthetic route is of great interest to materials scientists due to the capability of molecular level heating, which leads to homogenous and quick thermal reactions [12]. Microwave reactions have been used to prepare zinc sulphide but mostly these reactions require the use of pressurised containers made of quartz or Teflon [26–28].

Semiconductor photocatalysts have been established as viable materials for the creation of self-sterilising environments and for the destruction of bacteria. This self-sterilisation is an important part of combating healthcare associated infections, which are a serious problem at every level of healthcare systems [29]. The incidence of healthcare associated infections, HAIs is growing worldwide, especially the number of cases of methicillin-resistant *S. aureus* (MRSA) in Europe [30], North America [31], and Australasia [32,33]. This increase is mainly due to the epidemics of highly transmissible clones [34]. Studies have shown that prevention techniques such as cleaning and the use of barriers, gloves and gowns, can be effective but that behavioural practices limit the effectiveness of these methods [29]. This creates the need for a material on location which will create a sterile environment, and semiconductor photocatalysts are an ideal solution.

When the semiconductor is irradiated by a photon of light, which matches or exceeds the bandgap energy, E_g, an electron is promoted from the valence band to the conduction band leaving a positive hole. The photo-generated hole in the valence band and the photo-generated electron in the conduction band can serve respectively as oxidation and reduction species [35]. Titanium dioxide, TiO_2, is the most widely studied semiconductor photocatalyst has been shown to kill bacteria on its surface [36,37], has been incorporated into tiles to create self-cleaning surfaces [38] and into medical devices such as catheters [39]. The major advantage of using photocatalytic self-cleaning surfaces as a treatment for HAIs is that they operate in a passive manner, that is, without the need for chemicals or electric power, with only light, oxygen and water from the atmosphere required. The semiconductor surface is non-toxic and does not produce harmful by-products unlike some of the chemical reagents and cleaning products used as anti-bacterial agents [40].

In the current investigation, a novel ambient pressure microwave assisted method of producing zinc sulphide nanocrystals, which is a quick and straightforward water based reaction, where the product is collected and used as it is, is presented. The ZnS were characterised in detail and the anti-bacterial photocatalytic activities of these materials were tested against *E. coli*, and *S. aureus* and *P. aeruginosa.*

2. Experimental

2.1. Preparation of photocatalysts

In a typical synthesis, 200 mL of a 0.2 M zinc acetate dihydrate aqueous solution was added to 200 mL of a 0.2 M thiourea aqueous solution at room temperature. The beaker containing these solutions was placed in a MARS 5 microwave system and was irradiated at 600 W for 30 min under ambient pressure followed by a 5 min cool down period. After this time had elapsed the water had completely evaporated and a dry yellow powder was collected and characterised without further treatment. Samples prepared in this way are referred to by their irradiation power, *e.g.* ZnS450W – ZnS prepared at 450 W irradiation power.

2.2. Characterisation

The obtained ZnS was investigated using a combination of characteristic techniques including X-ray diffraction using a Siemens D 500 X-ray diffractometer with the diffraction angles scanning from $2\theta = 20–80^\circ$, using a Cu Kα radiation source. The diffuse absorbance spectra of the samples were measured by a UV–vis-NIR PerkinElmer Lambda 900 spectrometer between 800 and 200 nm with samples prepared in a KBr disc with a sample to KBr ratio of 1:10. Luminescence measurements were taken, with samples suspended in ethanol, by a PerkinElmer LS 55 luminescence spectrometer. X-ray photoelectron spectrometer measurements were taken with a Thermo VG Scientific (East Grinstead, UK) Sigma Probe spectrometer using a monochromated A1 Kα X-ray source ($h\nu = 1486.6$ eV), which was used at 140 W and the area of analysis was approximately 500 μm in diameter. Infrared spectra were obtained using a Spectrum GX Infrared Spectrometer. SEM images were obtained using a Hitachi SU-70 FE-SEM. Surface area measurements were measured using a Quantachrome Nova 2200 with the samples degassed at 300 °C for 2 h.

2.3. Anti-bacterial testing – agar test method

Agar plates were prepared using Mueller Hinton agar plate mix. The loading of the powder samples in the agar was 1% (w/w). The agar was autoclaved at 120 °C prior to testing. After autoclaving the agar was heated to 100 °C and the photocatalyst was added to the molten agar with stirring and dispersed with sonication before being poured onto a plate. Each of the agar plates were inoculated with 50 μL *E. coli*, 50 μL of *S. aureus* and 50 μL of *P. aerginosa* suspension. Each of these suspensions was diluted to approximately 1000 colony forming units/mL (CFU/mL). Each plate was prepared in triplicate with one sample irradiated with a 60 W light bulb (*i.e.* 3 plates irradiated) and one sample kept in the dark (*i.e.* three plates not irradiated). After irradiating the samples for 3 h with a 60 W light bulb, both sets of plates were placed in an incubator at 37 °C for 24 h to allow any growth of the bacteria to take place.

2.4. Anti-bacterial testing – suspension test method

The suspension test measures the bactericidal effect of the photocatalyst and makes it possible to determine a time frame for the reduction in the bacterial colonies. The reference sample for these tests contained no catalyst or powder. The reference sample consisted of 4.5 mL multi-recovery diluents, MRD, and is inoculated with 500 μL of 10^6 CFU/mL of bacteria. This gives a theoretical concentration of 10^5 CFU/mL at time zero. The test sample contains 10 mg of photocatalyst suspended in 4.5 mL of MRD, which was then inoculated with 500 μL of 10^6 CFU/mL of bacteria. The reference and sample both were exposed to light from a 60 W light bulb for a total of 5 h. Samples from both were taken at 0 min, 30 min, 1 h, 3 h and 5 h.

3. Results and discussion

The ZnS materials were prepared with microwave irradiation powers of 300, 450 and 600 W. In each preparation, a solution of zinc precursor and a solution of sulphur precursor were mixed in an open beaker. The solutions were irradiated in the microwave and at the end of the irradiation period of dry yellow powder was collected and used for all tests without further washing or synthesis steps. The simplicity of this reaction allows for the production of nanomaterials in a cost effective and easily scalable reaction scheme.

The solutions undergo dielectric heating upon irradiation in the microwave and the following mechanism is believed to lead to the formation of the zinc sulphide.

$$H_2NCSNH_2 + 2H_2O \rightarrow CO_2 + H_2S + 2NH_3 \quad (1)$$

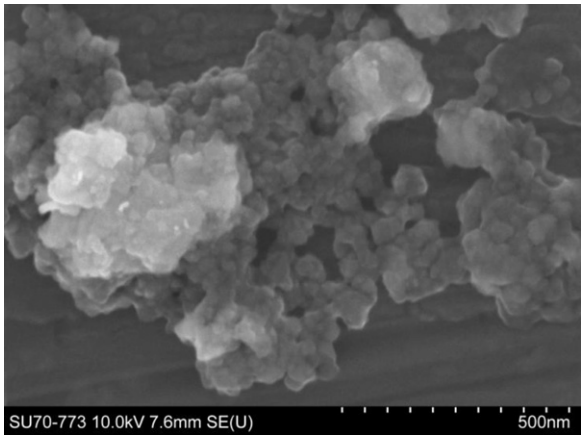

Fig. 1. SEM image of ZnS prepared at 450 W.

$$Zn^{2+} + H_2S \rightarrow ZnS + H_2 \quad (2)$$

In Eq. (1), the thiourea breaks down, at a temperature of 86 °C [41], forming H_2S, which is the sulphur source. The H_2S reacts with the liberated zinc ion from the zinc acetate solution, to form ZnS, Eq. (2). Zhao et al. [42] found that using zinc acetate as a precursor can lead to the ZnS agglomerating with the presence of the acetate. The acetate molecules interact with the surface of the ZnS crystals and cause the agglomeration. The agglomeration was investigated by SEM and infrared spectroscopy. The SEM images show agglomerations of ZnS particles, prepared at 450 W, of up to 100 nm in size (Fig. 1).

X-ray diffraction was employed to determine the crystal structure of the as-prepared powders. The peak pattern shows that all the samples prepared in the microwave are crystalline and sphalerite (cubic blende) phase zinc sulphide when compared to the International Centre for Diffraction Data (ICDD file #05-0566) [43,44] with the main peaks occurring at 28°, 47° and 56° corresponding to the (1 1 1), (2 2 0) and (3 1 1) planes respectively. (Fig. 3) The broadening of these peaks, demonstrate that the materials are nanosized, and calculations based on the Scherrer equation show all particles to be 4–6 nm in size (Fig. 2).

X-ray photoelectron spectroscopy was used to further clarify the identification of the material. The XPS spectra of ZnS450W (prepared in the microwave at 450 W irradiation power) is typical of the XPS data for the materials prepared (Fig. 3). The XPS spectra for the S 2p, Zn $2p_{1/2}$ and Zn $2p_{3/2}$ locates the peaks at 161.9, 1045.1 and 1022.1 eV respectively, which confirm the material as zinc sulphide [45,46]. It should be noted that the S 2p spectra are composed of

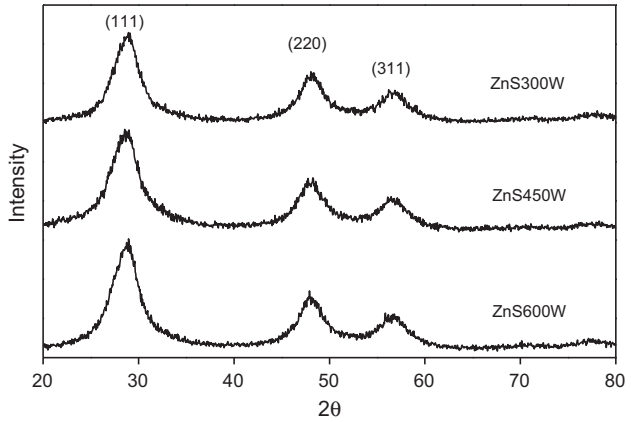

Fig. 2. X-ray diffraction spectra of ZnS samples prepared *via* microwave irradiation.

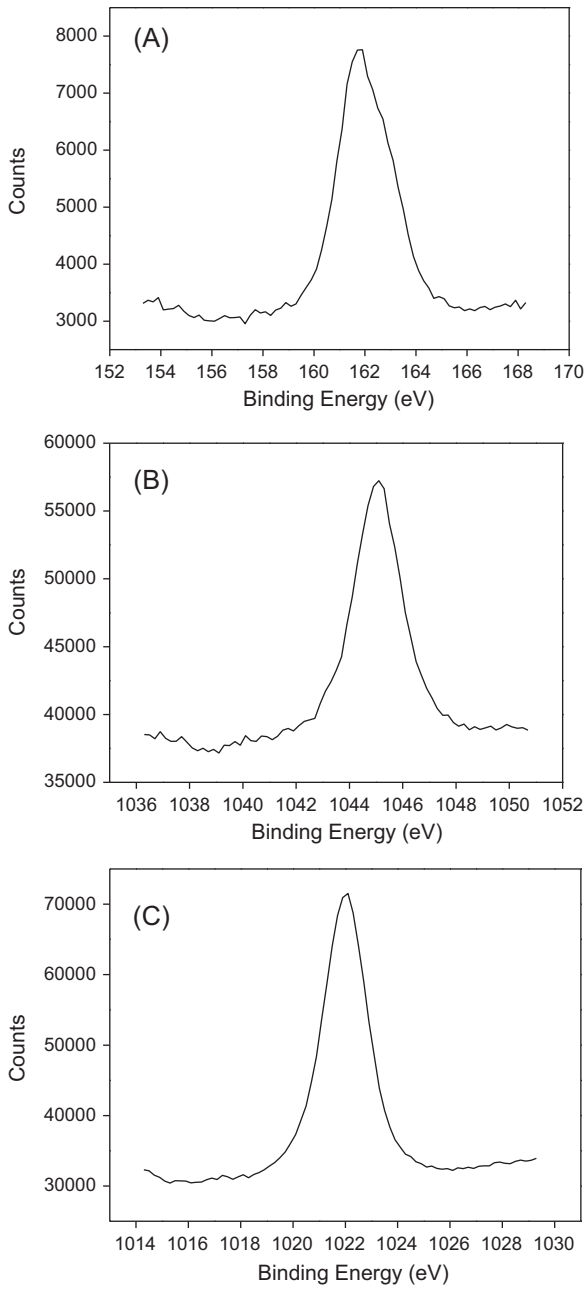

Fig. 3. X-ray photoelectron spectra of the (a) S 2p (b) Zn $2p_{1/2}$ (c) Zn $2p_{3/2}$ peaks of ZnS450W.

$2p_{3/2}$ and $2p_{1/2}$ peaks due to the spin–orbit splitting. Generally, the S $2p_{3/2}$ peak at lower binding energy is almost twice the intensity or area of the higher binding energy S $2p_{1/2}$ peak. These peaks are only around 1.1 eV apart and cannot be resolved from one another. The survey scan and more detailed scans indicate that there is no contaminants present on the surface of the material. The XPS spectra for the samples ZnS300W and ZnS600W are shown in supplementary information Figures 1 and 2 respectively.

The electronic properties of the as-prepared ZnS samples were investigated using a UV–vis spectroscopy (Fig. 4). The spectra for ZnS300W, ZnS450W and ZnS600W are shown, and it can be seen that the absorption edges from 320 to 340 nm which equate to band gaps of 3.8 to 4.0 eV. The band gap is greater than that of the bulk ZnS (3.7 eV) due to the quantum confinement effect associated with nanosized materials [47]. For these samples there is an absorption shoulder which extends to 420 nm and along with the yellow colour

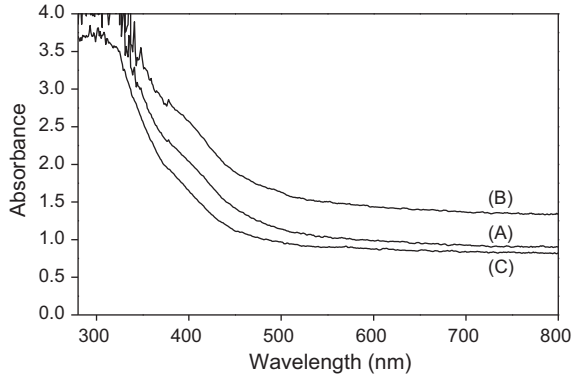

Fig. 4. Diffuse Absorbance spectra of (A) ZnS300W (B) ZnS450W and (C) ZnS600W.

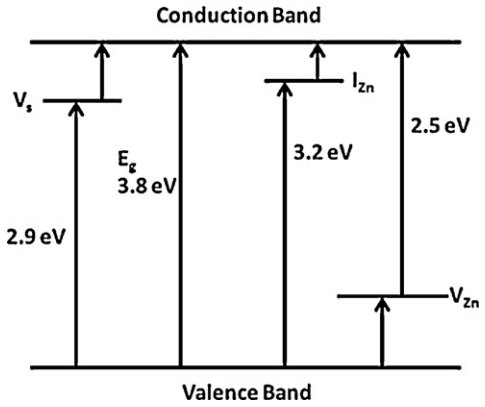

Fig. 6. Schematic energy level diagram of ZnS.

of the powder shows visible light absorption ($\lambda \geq 390$ nm). Luminescence spectroscopy offers an insight into the mechanism of the visible light absorption. The luminescence spectrum of ZnS450W was obtained upon excitation at 275 nm (Fig. 5). The peaks at 385, 427 and 489 nm correspond to three point defects within the ZnS crystal with the peak at 385 nm related to the interstitial Zn, the peak at 427 nm being from S vacancies and the peak at 489 nm relating to Zn vacancies [19,46]. These peaks and their related defects explain the visible light absorption as the levels of the defects act as donor levels within the band gap. Peng et al. [19] and others [48,49] showed that these defect sites can act as inter-band donor levels and reduced the energy required to promote an electron to the conduction band and leave a hole in the valence band, thus inducing photocatalysis. The luminescence spectra for the ZnS300W and ZnS600W are shown in supplementary information Figures 3 and 4 respectively. Based on these luminescence and absorption spectroscopy results, a schematic is proposed for the mechanism of visible light absorption. (Fig. 6) The donor levels, provided by the Zn and S vacancies, act as stepping stones for electrons travelling from the valence band to the conduction band. The donor levels energy gaps between the valance band and conduction bands are 2.5 and 2.9 eV respectively, which fall inside the region for visible light absorption. The main peak in the luminescence spectra at 385 nm which dominates the radiative decay lies inside the UV region of the spectrum.

The microwave prepared ZnS was tested for its anti-bacterial activity under irradiation from a visible light source. The ZnS (Table 1) sample tested was ZnS300W and three references were used, a blank, Degussa P25 TiO_2, a commercial photocatalyst standard and Sigma–Aldrich ZnS. Initial testing involved using 1% (w/w) of photocatalyst in agar and it was found that the ZnS

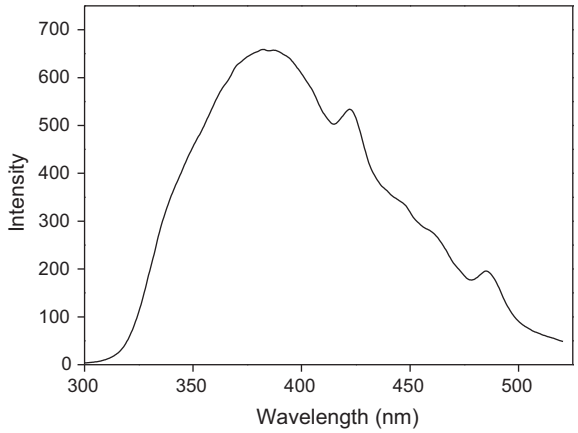

Fig. 5. Luminescence spectra of ZnS450W excited at 275 nm.

produced in the microwave had anti-bacterial properties in both light and dark conditions. The reference samples did not show any anti-bacterial properties as can be seen in Table 1. The agar plates were inoculated with both *E. coli* and *S. aureus* and it was found that the ZnS produced in the microwave prevented the growth of colonies of both of these bacteria. The reason for this is believed to be due to the small particle size of the ZnS and the high concentration of the photocatalyst in the agar, affecting the growth of the colonies. Fig. 7(a) shows agar plates with no photocatalyst, exposed to light and (b) the blank agar plate kept in the dark. Both plates show growth of *E. coli* and *S. aureus* bacterial colonies. Fig. 7(c) shows the plate loaded with 1% (w/w) of the ZnS300W photocatalyst to light and (d) the agar loaded with the photocatalyst kept in the dark. Both plates, Fig. 7 (c) and (d), show that no growth of the bacterial colonies of *E. coli* or *S. aureus* occurred. To determine the minimum inhibition concentration of ZnS required, to effectively prevent the growth of the bacterial colonies, plates containing 0, 0.25, 0.75% (w/w) ZnS300W were inoculated with *E. coli*, *S. aureus* and *P. aerginosa*. Each plate was exposed to light from a 60 W bulb for 3 h with a control plate for each concentration kept in the dark for the same time. After the irradiation time, the plates were kept overnight in an incubator at 37 °C. The plate containing no catalyst showed growth of all three bacteria in both light and dark conditions. At 0.25% (w/w) loading, in the dark conditions both the *S. aureus* and *E. coli* grew colonies, however on the plates exposed to light the growth of *S. aureus* was partially inhibited while the growth of *E. coli* colonies was fully inhibited. This is an indication of photocatalytic action against the bacteria by the microwave synthesised ZnS. At 0.75% (w/w) loading inhibition of *E. coli* and *S. aureus* bacteria was observed in both light and dark conditions, however the growth of *P. aerginosa*, a species resistant to many anti-bacterial agents, was not affected.

These tests showed that the ZnS acts as a bacteriostatic material preventing the growth of the test microbes in both light and dark conditions at concentrations above 0.75% (w/w) and that photocatalytic action takes place when the samples are exposed to light at concentration at low as 0.25% (w/w).

To observe the bactericidal effects of the material a suspension test was designed. The reference samples contained no catalyst and comprised of 4.5 mL of multi-recovery dilutent (MRD) and were inoculated with 500 μL of 10^6 CFU/mL of bacteria. The test samples contained 10 mg of ZnS300W suspended in 4.5 mL of MRD, which was inoculated with 10^6 CFU/mL of bacteria. This gave a concentration of 10^5 CFU/mL of bacteria in each sample. The reference and test samples were exposed to light from the 60 W bulb for 5 h with samples taken at 0 min, 30 min, 1 h, 3 h and 5 h and the concentration of bacteria was measured at each time point. Table 2 shows the concentration of bacteria at each time point for both the

Table 1
Colony growth of *S. aureus* and *E. coli* on agar plates loaded with 1% (w/w) photocatalyst.

Photocatalyst	Light exposure		No light exposure	
	S. aureus	*E. coli*	*S. aureus*	*E. coli*
Blank	Growth	Growth	Growth	Growth
Degussa-Evonik P25 TiO_2	Growth	Growth	Growth	Growth
Commercial ZnS (Sigma–Aldrich)	Growth	Growth	Growth	Growth
ZnS300W	No Growth	No Growth	No Growth	No Growth

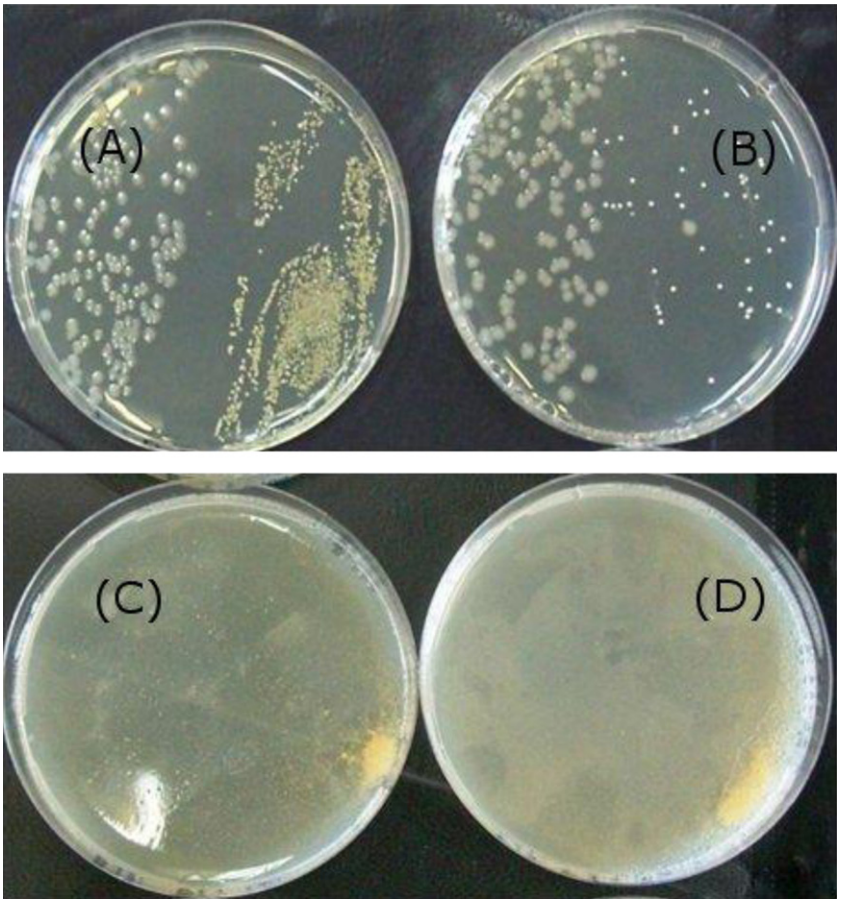

Fig. 7. (a) Blank agar exposed to light (L+), (b) blank agar kept in the dark (L−), (c) agar plate loaded with 1% (w/w) ZnS exposed to light (L+) and (d) the agar plate loaded with 1% (w/w) kept in the dark (L+).

reference and test sample and Fig. 8 shows a graph of the relative concentrations of bacteria. The test showed that there was an 88% reduction in the amount of bacteria in 5 h and showed the material to be bactericidal.

The study in this paper where the concentration of ZnS is varied and previous studies have shown that the anti-bacterial effect of the semiconductor is concentration dependant [1,50]. The increase in ZnS concentration leads to a decrease in the bacterial concentration, and in this study when the concentration was above 0.75% (w/w) of the agar, no bacterial colonies of *S. aureus* or *E. coli* were observed. It has been found that below the concentration threshold for which the ZnS is harmful to the bacteria that the number of bacterial colonies actually increases due to the fact that bacteria can metabolise Zn^{2+} at low concentrations [1]. A number of factors may play a role in the antibacterial effect of ZnS. *S. aureus* has an efflux mechanism for Zn^{2+} which suggests that free cations on the surface of the material generated by the photo dissociation of ZnS is toxic to the bacteria [51]. Oxidative species such as superoxide anions and singlet oxygen can be generated on the surface of the photocatalyst after irradiation with light [52] will also assist in the degradation of the cell membrane of the bacteria which leads to loss of cellular components and induces cell death [4,53]. The small size of the nanoparticle as shown by the broadening of the XRD peaks a larger surface area for contact with the bacteria also increases the antibacterial activity of the ZnS.

Table 2
Concentrations of the bacterial suspension test for the reference and test samples.

Time	0 h	0.5 h	1 h	3 h	5 h
Reference CFU count	8.7×10^5	5.8×10^5	6.7×10^5	1.4×10^6	2.2×10^6
Sample CFU count	5.8×10^5	2.7×10^5	2.2×10^5	1.5×10^5	7.3×10^4

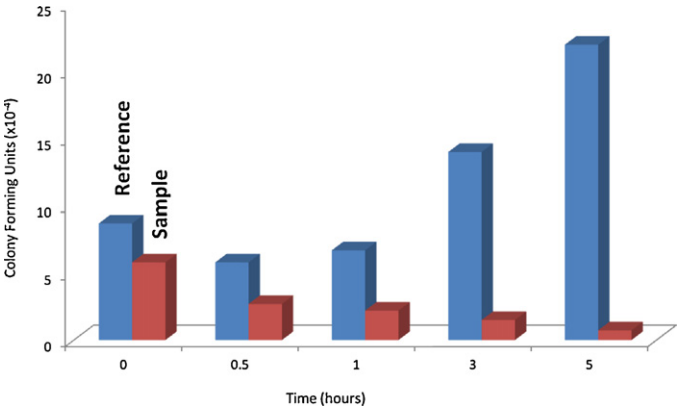

Fig. 8. Bacterial concentration of reference and ZnS300W sample to test the degradation rate of the photocatalyst.

4. Conclusions

In summary, a method of synthesising ZnS nanocrystals which is straight-forward, cost-effective and easily scalable has been created. The material produced is nanosized, crystalline and pure zinc sulphide with particles that are 4 nm in size. The material shows excellent antibacterial activity under irradiation from indoor light, conditions under which commercially available photocatalysts are inactive. The material is shown to be both photocatalytically bacteriostatic and bacteriocidal, preventing bacteria from growing on the surface and killing bacteria that are present. 88% of reduction in the concentration of bacteria was observed within 5 h of visible light irradiation. It was also observed that the increase in ZnS nanomaterial concentration leads to a decrease in the bacterial colonies and when the concentration was above 0.75% (w/w) of the agar, no bacterial colonies of *S. aureus* or *E. coli* were detected. It is envisaged that the small crystalline size and the high surface area of the ZnS nanoparticles are the major reasons for the significantly higher anti-bacterial activity compared to the commercial control samples. Luminescence spectroscopy reveals the possible mechanism of the indoor light activity with Zn and S vacancy defects acting as donor levels (2.5 and 2.9 eV) in the band gap allowing light in the visible region, up to 500 nm, to cause electron transfer from the valance band to the conduction band.

Acknowledgements

The authors wish to thank Science Foundation Ireland (SFI grant number 10/US/I1822) for supporting this investigation under the US-Ireland R&D partnership programme, CREST and Focas for lab and office facilities and equipment. The authors would also like to thank Dr. John Colreavy for reviewing the paper and providing valuable comments and Aisling Kirwan for providing the scanning electron microscopy images. The authors would like to acknowledge Enterprise Ireland Nanovigil (CFTD/06/IT/326 and ARE/2008/0005) for financial support.

Appendix A. Supplementary data

Supplementary data associated with this article can be found, in the online version, at http://dx.doi.org/10.1016/j.apcatb.2012.10.020.

References

[1] M. Pelaez, N.T. Nolan, S.C. Pillai, M.K. Seery, P. Falaras, A.G. Kontos, P.S.M. Dunlop, J.W.J. Hamilton, J. Byrne, K. O'Shea, M.H. Entezari, D.D. Dionysiou, Applied Catalysis B 125 (2012) 331.
[2] A. Kubacka, M. Ferrer, A. Martinez-Anas, M. Fernández-Garcia, Applied Catalysis B 84 (2008) 87.
[3] X. Hu, C. Hu, J. Qu, Applied Catalysis B 69 (2006) 17.
[4] A.G. Rincón, C. Pulgarin, Applied Catalysis B 49 (2004) 99.
[5] A.K. Benabbou, Z. Derriche, C. Felix, P. Lejeune, C. Guillard, Applied Catalysis B 76 (2007) 257.
[6] P.S.M. Dunlop, M. Ciavola, L. Rizzo, J.A. Byrne, Chemosphere 85 (2011) 1160.
[7] P.K.J. Robertson, J.M.C. Robertson, D.W. Bahnemann, Journal of Hazardous Materials 211 (2012) 161.
[8] J.A. Byrne, P.A. Fernandez-Ibanez, P.S.M. Dunlop, D.M.A. Alrousan, J.W.J. Hamilton, International Journal of Photoenergy, http://dx.doi.org/10.1155/2011/798051
[9] O.M. Alfano, D.W. Bahnemann, A.E. Cassano, R. Dillert, R. Goslich, Catalysis Today 58 (2000) 199.
[10] X. Fang, Y. Bando, M. Liao, U.K. Gautam, C. Zhi, B. Dierre, B. Liu, T. Zhai, T. Sekiguchi, Y. Koide, D. Golberg, Advanced Materials 21 (2009) 2034.
[11] S.H. Yu, M. Yoshimura, Advanced Materials 14 (2002) 296.
[12] Y. Wada, H. Yin, S. Yanagida, Catalysis Surveys from Japan 5 (2002) 127.
[13] X. Fang, Y. Bando, G. Shen, C. Ye, U.K. Gautam, M. Pedro, F.J. Costa, C. Zhi, C. Tang, D. Golberg, Advanced Materials 19 (2007) 2593.
[14] C. Feigl, S.P. Russo, A.S. Barbard, Journal of Materials Chemistry 20 (2010) 4971.
[15] D.D. Fanfair, B.A. Korgel, Crystal Growth & Design 8 (2008) 3246.
[16] L. Zepang, L. Bingbing, L. Xianglin, Y. Shidan, L. Wang, H. Yuanyuan, Z. Yonggang, M. Mingguang, L. Quanjun, Z. Bo, C. Tian, Z. Guantian, W. Guorui, L. Yichun, Nanotechnology 18 (2008) 255602.
[17] H. Zhang, J.F. Banfield, The Journal of Physical Chemistry C 113 (2009) 9681.
[18] J.H. Bang, R.J. Helmich, K.S. Suslich, Advanced Materials 20 (2008) 2599.
[19] W.Q. Peng, G.W. Cong, S.C. Qu, Z.G. Wang, Optical Materials 29 (2006) 313.
[20] E. Bacaksiz, O. Görür, M. Tomakin, E. Yanmaz, M. Altunbas, Materials Letters 61 (2007) 5239.
[21] C. Jiang, W. Zhang, G. Zou, W. Yu, Y. Qian, Materials Chemistry and Physics 103 (2007) 103.
[22] G. Feng, C.Z. Li, S.F. Wang, M.K. Lü, Langmuir 22 (2006) 1329.
[23] Y. Li, X. Li, C. Yang, Y. Li, The Journal of Physical Chemistry B 108 (2004) 16002.
[24] Y. Gou, Z. Su, Z. Xue, Materials Research Bulletin 39 (2004) 2203.
[25] G.Z. Wang, B.Y. Geng, X.M. Huang, Y.W. Wang, G.H. Li, L.D. Zhang, Applied Physics A 77 (2003) 933.
[26] T. Rath, Inorganic Chemistry 47 (2008) 3014.
[27] W. Jian, J. Zhuang, W. Yang, Y. Bai, Journal of Luminescence 126 (2007) 735.
[28] H. Yang, C. Huang, Y. Su, A. Tang, Journal of Alloys and Compounds 402 (2005) 274.
[29] S.W. Aboelela, P.W. Stone, E.L. Larson, Journal of Hospital Infection 66 (2007) 101.
[30] European Antimicrobial Resistance Surveillance System, Annual Report, 2003.
[31] D.J. Diekama, B.J. Bootsmillar, T.E. Vaughn, Clinical Infectious Diseases 38 (2004) 521.
[32] B.P. Howden, P.B. Ward, P.G.P. Charles, Clinical Infectious Diseases 38 (2004) 52.
[33] S. Kim, W. Park, K. Lee, Clinical Infectious Diseases 37 (2003) 794.
[34] I.M. Gould, Journal of Hospital Infection 61 (2005) 277.
[35] X.K. Li, S.X. Ouyang, N. Kikugawa, J.H. Ye, Applied Catalysis A: General 334 (2008) 51.
[36] A. Fujishima, K. Hashimoto, T. Wantanbe, TiO_2 Photocatalysis: Fundamentals and Applications, BKC Inc., Toyko, 1999.
[37] A. Fujishima, T.N. Rao, D.A. Tryk, Jounal of Photochemistry and Photobiology C 1 (2001) 1.
[38] T.N. Rao, A. Fujishima, D.A. Tryk, Applications of titanium dioxide photocatalysis, Chap. 19, in Encyclopedia on Electrochemistry, Vol. 6, Semiconductor Electrodes and Photoelectrochemistry (2002). A.J. Bard, M. Stratmann, S. Licht (Eds.), Wiley-VCH.
[39] K. Ohko, Y. Utsumi, C. Miwa, T. Tatsuma, K. Kobayakawa, Y. Saton, Y. Kubota, A. Fukishima, Journal of Biomedical Materials Research 58 (2001) 97.
[40] A. Fujishima, X. Zhang, D.A. Tryk, Surface Science Reports 63 (2008) 515.
[41] H. Shao, X. Oian, Z. Zhu, Journal of Solid State Chemistry 178 (2005) 3522.
[42] Y. Zhao, J.M. Hong, J.J. Zhu, Journal of Crystal Growth 270 (2004) 438.
[43] K.P. Subhendu, A. Dalta, S. Chaudhari, Chemical Physics Letters 440 (2007) 235.
[44] H. Zhang, Q. Li, Nanotechnology 17 (2006) 3984.
[45] C.M. Huang, K.W. Cheng, Y.R. Jhan, T.W. Chung, Thin Solid Films 515 (2007) 7935.
[46] M.V. Limaye, S. Gokhale, S.A. Acharya, S.K. Kulkarni, Nanotechnology 19 (2008) 415602.
[47] Y. Zhao, J.M. Hong, J.J. Zhu, Journal of Crystal Growth 270 (2004) 438.
[48] M. Scocioreanu, M. Baibarac, I. Baltog, I. Pasuk, T. Velula, Journal of Solid State Chemistry 186 (2012) 217.
[49] S.K. Mehta, S. Kumar, Journal of Luminescence 120 (2010) 2377.
[50] R. Brayer, R. Ferrari-Iliou, N. Brivois, S. Djediat, M.F. Benedetti, F. Fievet, Nano Letters 6 (2006) 866.
[51] K.M. Reddy, K. Feris, J. Bell, D.G. Wingett, C. Hanley, A. Punnoose, Applied Physics Letters 90 (2007) 213902.
[52] M. Pelaez, P. Falcras, V. Likodimos, A.G. Kontos, A.A. De la Cruz, K. O'Shea, D.D. Dionysiou, Applied Catalysis B 99 (2010) 378.
[53] J. Kiwi, V. Nadtochenko, Langmuir 21 (2005) 4631.